Results in Chemistry 4 (2022) 100345

Contents lists available at ScienceDirect

Results in Chemistry

journal homepage: www.sciencedirect.com/journal/results-in-chemistry

Immunosuppressive drug sensor based on MoS_2-polycarboxyindole modified electrodes

Vineet Kumar Mall, Ravi Prakash Ojha, Preeti Tiwari, Rajiv Prakash *

School of Materials Science and Technology, Indian Institute of Technology (BHU), Varanasi 221005, India

ARTICLE INFO

Keywords:
Immunosuppressive
Poly(5-carboxyindole)
MoS_2 nanosheets
Electrocatalytic

ABSTRACT

Azathioprine (Azp) is the principal immunosuppressive drug used in organ transplantation autoimmune diseases by improving therapeutic management and suppressing the immune system. Any discrepancy of Azp in human blood may lead to some serious side effects that obligate its quantitative estimation. In this work, the molybdenum disulfide (MoS_2) nanosheets modified with poly(5-carboxyindole) (CPIn) is reported for quantitative estimation of Azp. The synthesis of MoS_2 nanosheets is reported through single-step one-pot hydrothermal reaction and exfoliation of sheets is obtained in an aqueous dispersion of 5-carboxyindole (5CIn) through probe ultra-sonication. The nanosheets are further utilized as a template for the growth of the poly(5-carboxyindole) to obtain CPIn stabilized MoS_2 nanosheets (MoS_2-CPIn). The synthesis of MoS_2-CPIn nanohybrid is further validated via different characterization techniques including FTIR, XRD, SEM, TEM, and XPS. MoS_2-CPIn with magnificent electrocatalytic property is further exploited for the electroanalytical sensing of Azp via Differential Pulse Voltammetry (DPV) in phosphate buffer solution at biological pH (pH = 7.4) as well as human blood serum at room temperature. The proposed sensor shows a linear dependence of current with Azp concentration. The developed sensor demonstrates an extensively wide linear range of 3.49–284.44 μM possessing a low limit of detection of 74.65 nM (S/N = 3). The developed sensor shows excellent stability, sensitivity, and good selectivity in physiological pH. The achieved analytical parameters of the proposed sensor for easy quantification of Azp are found to be comparable or better than the previously reported Azp sensors and it is proved to be an excellent contestant for the trace level estimation of Azp in human blood serum.

1. Introduction

Azathioprine (Azp) is associated with a chemical category of purine analogues named 6-[(1-methyl-4-nitroimidazole-5-yl) thio] purine. Azp is an immunosuppressant and antileukemic drug that finds contemporary applications in various disorders such as ulcerative colitis, rheumatoid arthritis, Crohn's disease, and pemphigus [1,2]. Mercaptopurine is the active form of Azp which acts by decreasing the reactions of T and B cells by inhibiting their proliferation [3]. The continued exposure of Azp for a long time may lead to the development of specific types of cancer like skin cancer, blood cancer, and lymphoma and with some serious side effects including hair loss, nausea, fatigue, and rash. In order to counter these issues, it is crucial to evolve an accurate and sensitive method for the routine and careful monitoring of Azp in clinical operations [4,5]. In past, various techniques have been applied, for instance, high performance liquid chromatography (HPLC) [6,7], UV–Visible spectrophotometry [8,9], ^{1}H NMR spectroscopy [10], chemiluminescence [11,12], ultra-performance liquid chromatography [13], high performance thin layer chromatography [14], flow injection analysis [11], surface-enhanced Raman spectroscopy [15], capillary zone electrophoresis [16], titrimetry [17] for the determination of Azp in human blood. Although all these techniques are accurate, some of them suffer from various demerits like low sensitivity and selectivity, expensive instrumentation, high cost, time-consuming operation, cumbersome extraction procedure with complex and tedious sample pretreatment that makes them inappropriate for regular analysis in many cases. Analytical and electrochemical measurement techniques play a critical role in biological recognitions, environmental monitoring, and drugs estimation in human body fluids as well as pharmaceutical formulations. The modern electrochemical methods have an important role in these fields because they have come up with sensational advantages like broad linear dynamic range, high sensitivity, and selectivity, simplicity, short analysis time, cost-effectiveness with real-time monitoring [18–20]. Cyclic Voltammetry (CV) [21] and Differential Pulse

* Corresponding author.
E-mail address: rprakash.mst@iitbhu.ac.in (R. Prakash).

https://doi.org/10.1016/j.rechem.2022.100345
Received 12 February 2022; Accepted 17 April 2022
Available online 20 April 2022

Voltammetry (DPV) [22] have enjoyed a significant interest since they can be used for elucidation of redox electrode process and estimation of trace level amounts of electroactive analytes respectively. The electroreduction of Azp on bare glassy carbon electrode (GCE) displays an inadequate and wide signal unveiling high overpotential magnitude. Also, this involves very slow electron transfer kinetics [22]. These issues can be addressed and the electrode kinetics can be enhanced through surface modification using a mediator which can fasten the transfer of electrons thereby amplifying the sensitivity and selectivity of the analysis. To serve this purpose, nanostructured materials like nanoparticles [23,24], nanosheets [25–27], nanotubes [28,29], etc. present themselves as promising candidates due to their small dimension and size with shape-dependent properties [30,31]. Recently, two-dimensional layered nanomaterials (2D nanomaterials) like graphene, transition metal dichalcogenides (TMDs), and other analogs have attained great privilege towards application in the field of electrochemistry. Molybdenum disulfide (MoS_2) categorizes a typical two-dimensional transition metal dichalcogenides, which can be easily exfoliated to a few layers because of the weak van der Waals interactions. MoS_2 shows several properties similar to graphenes like easy functionalization, large surface area, good mechanical strength, and easy storage. Owing to these properties, MoS_2 has found wide applications in the field of electronic devices, electrochemical sensors, catalysis, energy storage [32–37]. For augmenting the electrical, thermal, and mechanical properties, MoS_2 are further modified with different metal nanoparticles, carbonaceous materials, and conducting polymers [38,39]. Among them, conducting polymers are an excellent choice of materials for modification because of their low cost, commendable conductivity, and rapid redox kinetics [40]. But only a few works have been reported on the modification of MoS_2 with conducting polymers [41–44]. Among conducting polymers, polyindole (PIn) is a promising material to serve the purpose of electrode materials since it combines the properties of polyphenylene and polypyrrole. They display advantageous properties like low toxicity, high redox activity, high thermal stability, fast electrochromic response, and great environment stability. In addition, poly(5-carboxyindole) (CPIn) displays a unique property of pH-dependent self-doping due to the presence of COO^- and demonstrates rapid electron transfer [45].

In the current study, MoS_2 has been synthesized using a simple single-step hydrothermal process that provides good control over size and morphology. These MoS_2 nanosheets were further exfoliated in an aqueous medium using monomer 5-carboxyindole (5CIn) without any aid from hazardous solvents and chemicals. These exfoliated nanosheets were exploited as templates for the controlled polymerization of 5CIn using ammonium persulphate (APS). The as-prepared Poly(5-carboxyindole) stabilized MoS_2 nanosheets (MoS_2-CPIn) composite was characterized by numerous techniques, for instance, FTIR, XRD, SEM, TEM, EDAX, and their electrochemical properties were investigated by voltammetry. MoS_2-CPIn showed commendable electrocatalytic activity and is therefore used as a nano mediator over GCE surface for electrochemical sensing of immunosuppressive drug Azp. The work demonstrates a simple, sensitive, selective, and low-cost sensory platform with a large surface area for trace level detection of Azp.

2. Experimental

2.1. Materials and methods

Azp, 5CIn, Ammonium persulfate (APS; $(NH_4)_2S_2O_8$), L-Cysteine ($HO_2CCH(NH_2)CH_2SH$), Sodium molybdate dihydrate ($Na_2MoO_4{\cdot}2H_2O$), Hydrochloric acid (HCl), sodium dihydrogen phosphate (NaH_2PO_4), disodium hydrogen phosphate (Na_2HPO_4) were purchased from Merck, India. Chemicals used in the interference study i.e. L-ascorbic acid, cholesterol, creatine, dopamine, glucose, glycine, uric acid, and urea were procured from Sisco Research Laboratories Pvt. Ltd., India. The 0.1 M phosphate buffer solution (PBS) was formulated by intermixing NaH_2PO_4 and Na_2HPO_4. The Deionized (DI) water was utilized in every preparation and experiment. Blood serum sample was collected from Sir Sundar Lal Hospital, BHU for Azp detection in human blood serum.

2.2. Preparation of MoS_2 nanosheets

A hydrothermal one-step reaction was employed for synthesizing MoS_2 nanosheets (MoS_2) (Scheme S1) [44]. Cysteine (0.5 g) and sodium molybdate dihydrate (0.25 g) were added to DI water (25 mL) in different beakers and constantly stirred for 30 min to get a complete homogenous solution. Then, both the solutions were intermixed and agitated well for 30 min with temperature maintained at ~40 °C and conc. HCl (12 N) was added to maintain the pH at 3. The prepared reaction mixture was introduced into a stainless-steel Teflon-coated autoclave (100 mL) and retained at 200 °C for ~42 h. The reaction mixture was further cooled down to room temperature (RT), the dark brown precipitate was obtained by centrifugation. The product was washed with DI water 4–5 times repeatedly followed by washing with ethanol and the product was finally vacuum dried at 80 °C overnight.

2.3. Synthesis of MoS_2-CPIn composite

MoS_2-CPIn composite has been synthesized as per reaction scheme S2. For that, 10 mg MoS_2 was suspended in 10 mL 0.1 N HCl and sonicated properly to achieve uniform distribution. 20 mg of 5CIn monomer was solubilized in a minimum amount of ethanol and was mixed dropwise in MoS_2 suspension. The mixture was constantly stirred for 1 h, further sonicated using probe sonication so that monomer gets completely adsorbed over nanosheets and restrict further stacking of nanosheets. 28.32 mg APS was dissolved in 0.1 N HCl (5 mL). This solution was mixed dropwise in the prepared suspension with subsequent stirring for polymerization. The reaction was then kept in the refrigerator overnight. After 24 h, the precipitate was extracted by centrifugation at 5000 rpm and washed three times with ethanol to eradicate the unreacted monomer. Later, the product was vacuum dried at 60 °C and preserved in the desiccator.

2.4. Instrumentation

MoS_2 synthesis was carried out in a hydrothermal autoclave reactor (Hydrion Scientific Instruments, USA). MoS_2, CPIn, and MoS_2-CPIn composite were characterized by several characterization tools. Absorbance studies were performed using a UV–Vis spectrophotometer (UV-2600, Shimadzu). FTIR (Thermo 5700 FT-IR spectrometer, Germany) was used for structural analysis. Morphological studies were performed through SEM micrographs (EVO|18 Zeiss Model at an operating voltage 20.0 kV). XRD evaluation of synthesized compounds was recorded by Rigaku MiniFlex Benchtop 600 X-ray diffractometer, CuKα (Kα = 1.54056 Å) at a rotational speed of 3° min^{-1} with 2θ ranging from 5° to 80°. TEM micrographs of the materials were recorded on a carbon-coated copper grid using HR-TEM (FEI, Technai G2 20 TWIN, Czech Republic) at an accelerating voltage = 200 kV. Elemental analyses were investigated by X-ray spectroscopy on Kratos Analytical Instrument, Shimadzu, Amicus XPS, UK. Every electrochemical measurement of CV and DPV was recorded using Metrohm Autolab (PGSTAT, 302, The Netherlands, NOVA 1.11 software) with a conventional cell system of three electrodes. MoS_2-CPIn coated glassy carbon electrode, Pt electrode, Ag/AgCl were selected as working, auxiliary, and reference electrodes respectively. Azp detection was executed in a 0.1 M PBS buffer of pH 7.4. DPV parameters were optimized for the best analytical signal. DPV parameters such as the potential window of 0.0 V to 0.9 V, step potential of 5 mV, modulation amplitude of 25 mV, modulation time of 50 ms, and interval time of 500 ms was chosen to obtain the best signal.

3. Results and discussion

3.1. Structural investigation

The crystallographic nature of the as-synthesized composite was examined through the XRD technique. The XRD measurements of CPIn, MoS_2, MoS_2–CPIn composite are demonstrated in Fig. 1 (a). Pure CPIn displayed diffraction peaks with characteristic weak reflections between 15 and 30° [44]. MoS_2 showed XRD signals positioned at $2\theta = 13°$, 33°, 35°, 44°, and 58° which may be observed due to the presence of (002), (100), (103), and (110) planes which are directly related to MoS_2 hexagonal phase (JCPDS No. 37-1492) [44,47]. MoS_2-CPIn composite shows the signature of both CPIn and MoS_2 and has diffraction peaks with decreased intensity and increased FWHM due to growth of the polymer over MoS_2 sheet that restricts restacking of the sheet, this fact is well supported by TEM analysis (Fig. 1(g-i)). The star (*) in the XRD spectra indicates the peak corresponding to the glass which was used as a substrate for recording spectra.

The FTIR spectroscopy has been done for the structural investigation of CPIn, MoS_2, and MoS_2-CPIn. Fig. 1 (b) depicts the FT-IR spectra of CPIn, MoS_2, MoS_2-CPIn. MoS_2 exhibits signals at 1612 and 1673 cm^{-1} that correspond to in-group deformation of NH_2 and -C=O vibrational stretching (due to L-cysteine used as a reactant in hydrothermal synthesis), and the peak observed at 1407 cm^{-1} can be accredited to the asymmetric N–C–N vibrational stretching mode. The O–H stretching vibration band appeared at 1185 cm^{-1} and the vibrational peak appeared at 1108 cm^{-1} corresponding to the C–O–H stretching vibration. The C-S vibration stretching is detected at 899 cm^{-1}. A small peak is observed near 670 cm^{-1} which reflects Mo–S vibration [46]. The CPIn exhibits characteristic peak for aromatic rings at 765 cm^{-1} (corresponding to C–H bond out of plane deformation in the benzene moiety), 1228 cm^{-1} with 1677 cm^{-1} (representing the distinguishing absorption peak for -C-O and -C=O corresponding to the vibration stretching modes of –COOH), 1377 cm^{-1} (assigned to C-O–H bonds in the plane shearing mode of vibration), 1612 cm^{-1} (vibrational stretching of -C=C group present in indole ring) [47]. The characteristic vibrational peaks for both Mo–S and CPIn are consistently observed in MoS_2-CPIn composite.

The elemental composition of synthesized MoS_2-CPIn was investigated using XPS. Fig. 1(c) depicts the XPS survey of MoS_2-CPIn signifying the existence of all elemental compositions. Fig. S.1(a) shows the C 1 s XPS spectrum of MoS_2-CPIn that may be deconvoluted into four peaks: 284.8 eV, 286.8 eV, 288.8 eV, 290.7 eV designated to C–C/C = C, C = N, C–N and (O–C = O) respectively signifying various kinds of carbon present in the composite. Fig. S.1(b) shows the XPS spectrum of N 1 s with a prominent signal at 399.9 eV which corresponds to the pyrrolic N (5CIn) in the composite [48,49].

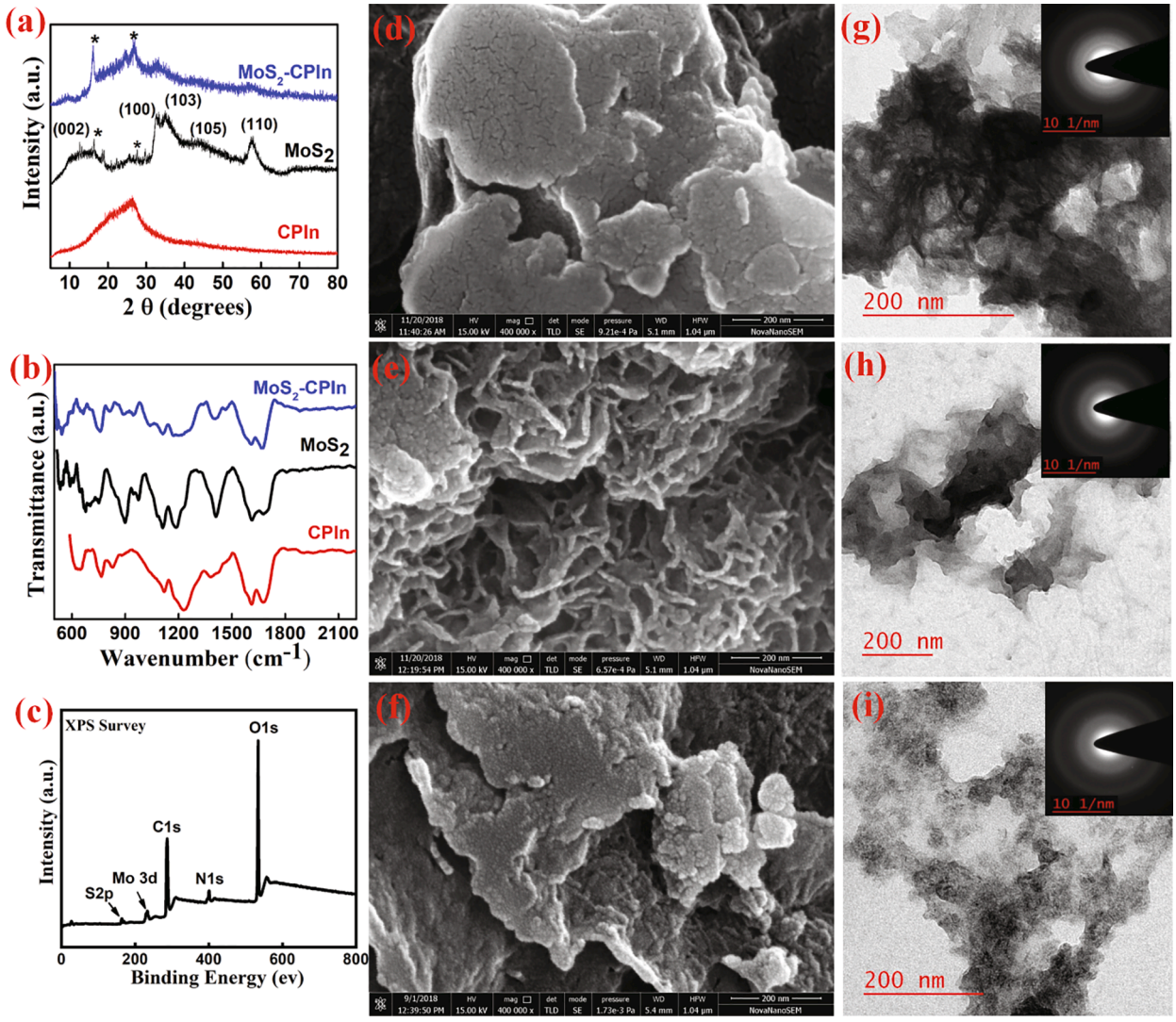

Fig. 1. (a) XRD spectrum of MoS_2, CPIn and MoS_2-CPIn, (b) FTIR spectra of MoS_2, CPIn and MoS_2-CPIn, (c) XPS survey spectrum corresponding to MoS_2-CPIn (d) displays the SEM image related to CPIn, (e) MoS_2 and (f) MoS_2-CPIn, (g) TEM micrograph of MoS_2, (h) CPIn and (i) MoS_2-CPIn, Inset of g-i shows SAED pattern.

Fig. S.1(c) displays the XPS spectrum of O 1 s which may be deconvoluted into two peaks at 533.2 eV (C-O) and 531.6 eV (C=O) designating two different types of oxygen present [50]. The XPS spectrum of Mo 3d region (Fig. S.1(d)) may be further deconvoluted into 6 peaks. The XPS signals at 226.7 eV is designated to S 2 s of MoS_2 and an intense peak is observed for Mo (IV) $3d_{5/2}$ and Mo (IV) $3d_{3/2}$ binding energies at 228.8 eV and 232.0 eV respectively. Short peaks observed at 233.2 eV and 235.9 eV are designated to Mo $3d_{5/2}$ and Mo $3d_{3/2}$ of Mo (VI) indicating that Mo (IV) is partially oxidized to Mo (VI) during hydrothermal-assisted preparation of MoS_2. Fig. S.1(e) shows a deconvoluted XPS spectrum related to S 2p peak. The signals examined at 163.7 eV corresponds to S $2p_{1/2}$ and 161.8 eV is the signature of S $2p_{3/2}$ for S^{2-} [51,52]. The morphology of the developed composite MoS_2-CPIn was assessed using SEM. Fig. 1(d) represents the SEM micrograph of CPIn designating sheet-like morphology. Fig. 1(e) shows the pure MoS_2 having flower-like morphology, consisting of interlaced nanosheets. SEM image reveals that the MoS_2 nanosheets are well rough, porous, and scattered. Fig. 1(f) shows the growth of the CPIn chain in between and over the MoS_2 sheets. MoS_2 sheets provide a good structural substrate for the growth of CPIn polymer chains. TEM micrographs of MoS_2 (Fig. 1g), CPIn (Fig. 1h), MoS_2-CPIn (Fig. 1i) were used to demonstrate the internal nature of the developed composite. MoS_2 nanosheets are covered by homogeneously distributed CPIn chains and these chains are very well anchored on the nanosheets. So, the TEM study strongly supports the composite formation. SAED pattern displays the ring-like structure which confirms the polycrystalline nature of the MoS_2 nanosheets.

4. Electrochemical sensing of Azathioprine

4.2. Electrode fabrication

Initially, the GCE with a diameter 3 mm was cleaned by polishing it in 0.3 μm alumina slurry. Further, it was undergone through 2 min sonication in DI water followed by acetone three times and dried in a desiccator. The MoS_2-CPIn composite (1.0 mg) suspension in DI water (1 mL) was sonicated for 1 hr to yield a homogeneous suspension. Further, 5 μL of prepared ink was used to modify the polished GCE surface by using the drop-casting technique and followed by vacuum drying in a desiccator. MoS_2-CPIn acts as a good electrode modifier because they are negligibly soluble in water so that the factor of leaching of the material from the electrode surface can be eliminated.

4.3. Electroanalytical response of Azp at MoS_2-CPIn/GCE

Azp is an aromatic compound that is electroactive due to the presence of a nitro group (–NO_2). CV of 9.9 μM Azp was recorded on modified MoS_2-CPIn/GCE in PBS buffer from 0.0 to −0.9 V potential window at a scan rate of 50mVs^{-1} (Fig. S2) to investigate the electrochemical response of Azp. A sharply defined cathodic peak was observed at −0.656 V in the forward scan and a small anodic peak was found at −0.563 V during the reverse scan. The cathode peak can be attributed to the nitro group (–NO_2) reduction to hydroxylamine (–NHOH) which is irreversible and anodic peak can be assigned to the reversible conversion of the hydroxylamine group to nitroso group as shown in the equation below [53]. The electrochemical reduction of the nitro group involves complex mechanisms and the cathodic peak is ascribed to the 4-electron process in which nitro group is reduced to hydroxylamine group (–NHOH). This is in accordance with previously reported works on the electro-reduction of nitro aromatic compounds. For instance, the redox behavior of –NO_2 group was explored previously by Zen *et al* and Chen *et al* during voltammetric estimation of chloramphenicol and parathion respectively [54,55]. Further, the redox process at bare electrode involves very slow electron kinetics and hence it requires an appropriate electron mediator on the electrode surface for catalytic improvement. On the surface of bare GCE, a very poor and broad cathodic peak of Azp is observed due to very slow electron transfer kinetics. The modification of GCE with a suitable electron nano-mediator results in improved electrocatalytic activity and the enhanced voltammetric response of Azp. The voltammetric response was enhanced because of Azp adsorption over the composite surface via π-π interaction between the benzene rings of Azp and MoS_2-CPIn. So, the electrochemical behavior of the Azp can be showcased by the following chemical equation:

4.4. Optimization of supporting electrolyte pH

CV (Fig. 2a) and DPV (Fig. 2b) of 9.9 μM Azp were performed in PBS buffer of different pH (pH = 6.4, 7.0, 7.4 and 8.0) for optimization of pH. The reduction peak current enhances on moving from pH 6.4 to 7.4 and decreases from pH 7.4 to 8.0. This dependency of the Azp reduction peak current over the pH is attributed to the crucial role of protons in the electrochemistry of Azp [53]. So, the supporting electrolyte was decided to be PBS buffer of pH 7.4 at which the maximum current is obtained as a result of the enhanced catalytic activity of the proposed material.

4.5. Comparison of different modified electrodes for Azp detection

The MoS_2-CPIn modified GCE did not display any redox peak within the selected potential window (0.0 to −0.9 V) *vs.* Ag/AgCl for the blank test sample. So, a suitable potential window was selected such that no redox peak of the material was observed in this range. Electrodes of bare, MoS_2, CPIn, and MoS_2-CPIn modified GCEs were thoroughly investigated for voltammetric responses of 50 μM Azp in PBS buffer of pH 7.4 through CV (Fig. 3 a) and DPV (Fig. 3 b). It is clearly observed that reduction occurs at the same potential in all the considered cases but the peak current gets varied after different modifications and the current intensity was observed in sequence: Bare < CPIn < MoS_2 < MoS_2-CPIn under identical conditions. The result indicates that the composite formed has shown synergism between individual components. In addition, it has a huge surface area and the ability to amplify the electrocatalytic activity of the nanomaterial and it shows remarkable conductivity.

4.6. Voltammetric sensing of Azathioprine

Under all the optimized conditions, voltammetric experiments were performed for investigating the analytical performance of MoS_2-CPin towards Azp detection using the DPV technique. Upon successive additions of Azp, well-defined voltammetric responses were recorded in PBS buffer as shown in Fig. 4 (a). On successive addition of Azp, a substantial increment in the reduction peak current depicts a rapid electron transfer reaction over the MoS_2-CPIn modified electrode, owing to the excellent catalytic effect of the nanostructured platform. The calibration plot in PBS buffer was prepared between Azp concentration and reduction peak current (Fig. 4b). Thus, our sensing platform is extremely sensitive towards Azp estimation and displays a linear current response with a concentration in an extensive range from 3.49 μM to 284.44 μM. The linear regression equation was evaluated as Ipc (Azp) = 0.02379C + 1.55493 with the correlation coefficient R^2 = 0.99. The sensitivity and limit of detection of Azp over MoS_2-CPIn modified GCE using DPV technique was determined as 0.33986 μA·μM^{-1}·cm^{-2} and 74.65 nM respectively.

Detection of Azp in human blood serum is of utmost significance to assess the practicability of the modified electrode for the analyte so that it can be used in diagnostic centers in the future. For this analysis, blood samples were obtained from a healthy person and blood cells are eliminated through centrifugations leaving behind the serum. This serum sample is diluted 10 times using PBS buffer (pH 7.4; 0.1 M). The pH was again checked after dilution in order to assure the final pH of the solution was 7.4. This sample solution did not display any reduction peak at MoS_2-CPIn modified GCE thereby indicating the absence of any reducible compound within the selected potential window. Now, the

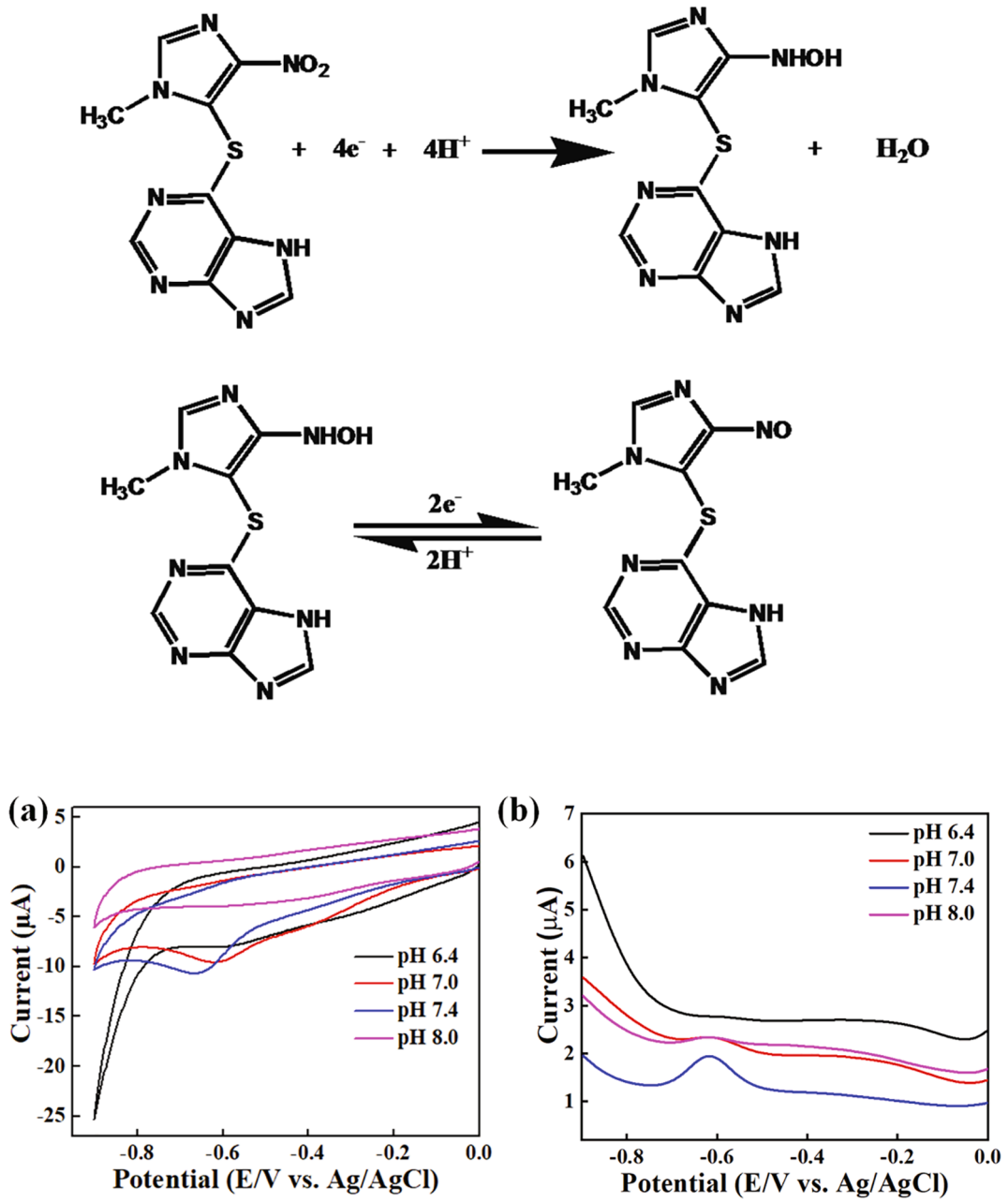

Fig. 2. (a) CV of Azp (9.9 μM) in 0.1 M PBS buffer over MoS_2-CPIn modified GCE at different pH 6.4, 7.0, 7.4 and 8.0, (b) DPV of Azp (9.9 μM) in 0.1 M PBS buffer over MoS_2-CPIn modified GCE at different pH 6.4, 7.0, 7.4 and 8.0.

electrochemical sensing behavior using DPV technique was investigated at the modified GCE in the concentration window of 4.00 μM to 98.29 μM and a linear calibration plot was observed (as shown in Fig. 4 (c) & (d)) with a detection limit of 195.89 nM with 0.29557 $\mu A \cdot \mu M^{-1} \cdot cm^{-2}$ sensitivity (S/N: 3). Now, the detection of Azp was investigated in spiked human serum samples using a similar dilution procedure and PBS buffer of pH 7.4. The recovery study of the developed sensor has been investigated using the standard addition method. The standard solution of Azp was added into the test solution and the calibration plot was utilized for the quantitative estimation of Azp. The results obtained from three serum samples are listed in Table 1 and values demonstrate a good recovery of results. The proposed sensor with obtained results of the analytical parameters was compared with that of the previously reported Azp sensors and presented in Table S1. The observed results suggest that the proposed sensor can effectively be used for the quantitative estimation of Azp in the real sample analyses.

4.7. Selectivity and interference study of the proposed sensor

While designing a sensor, selectivity and cross-reactivity studies are of utmost importance because complex test samples contain many other bio components like lipids, carbohydrates, etc. that can hinder the detection of the desired analyte. So, the selectivity of our proposed sensor for Azp detection was investigated with some common biologically important molecules that are present in human blood like L-ascorbic acid, cholesterol, creatine, dopamine, glucose, glycine, uric acid and urea and as shown in Fig. 5. The concentration of all the interferants was chosen 10 times higher than the Azp concentration. The percentage interference was calculated to be 5.39 % for L-ascorbic acid, 7.87 % for cholesterol, 2.99 % creatine, 3.14 % for glucose, 4.33 % for glycine, 9.88 % for urea, 5.85 % for uric acid, and 12.79 % for dopamine respectively and clearly, all of them showed very less or negligible interference. It was clearly demonstrated that our proposed

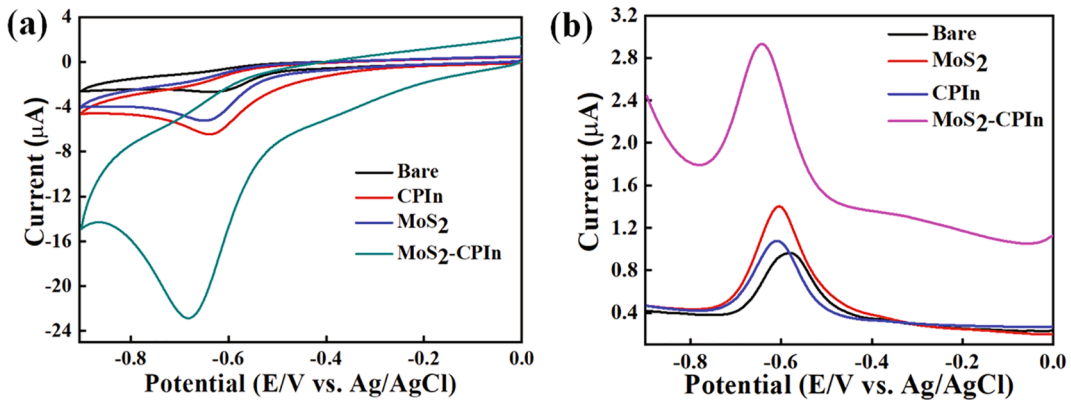

Fig. 3. (a) CV plots of Azp (50 μM) in PBS buffer (pH 7.4; 0.1 M) over different electrodes, (b) DPV curves of Azp (50 μM) in PBS buffer (pH 7.4; 0.1 M) over different electrodes.

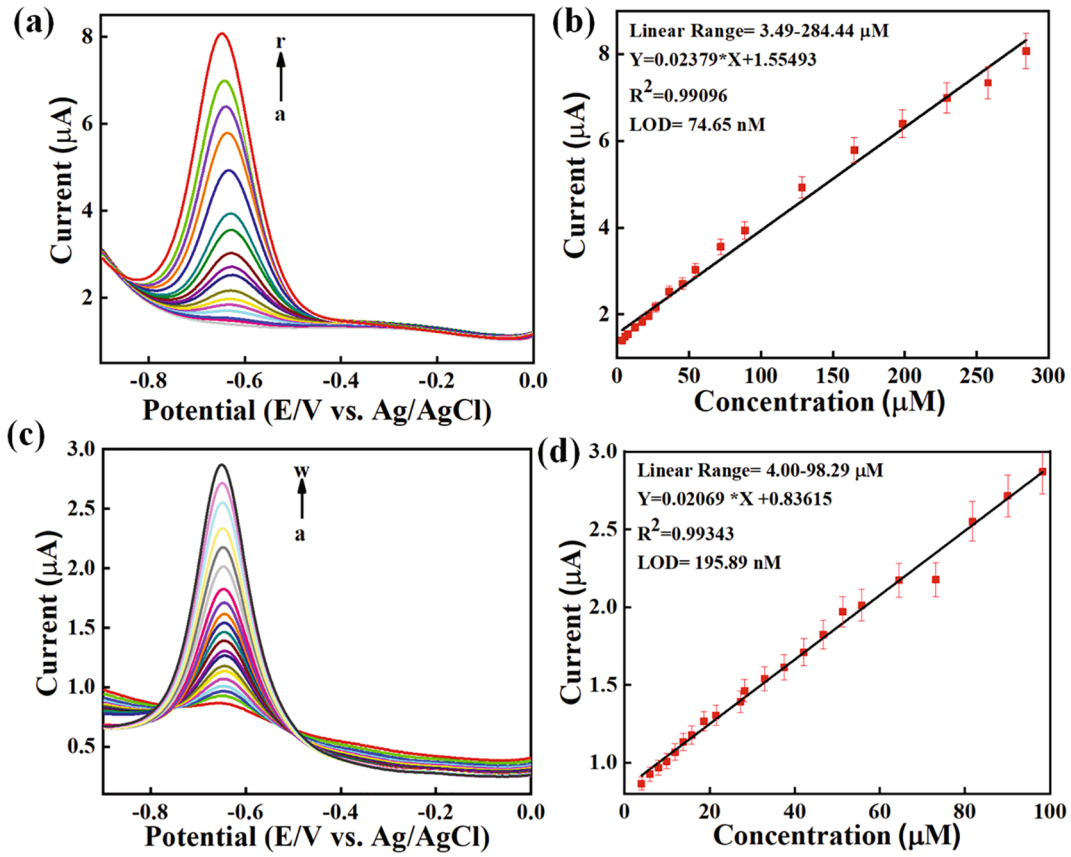

Fig. 4. DPV measurements of various concentrations of Azp (3.49–284.44 μM) (a-r) using MoS_2-CPIn modified GCE in PBS buffer (pH 7.4; 0.1 M), (b) linear calibration plot of Azp in PBS buffer (pH 7.4; 0.1 M). (c) DPV responses of different concentrations of Azp (4–98.29 μM) (a-r) using MoS_2-CPIn modified GCE in human blood serum, (d) linear calibration plot of Azp in the human blood serum sample.

Table 1
DPV detection of Azp in spiked blood serum sample.

Blood Serum Samples	Spiked (μM)	Detected* (μM)	Recovery (%)
Sample A	11.80	11.40	96.61
Sample B	46.75	47.78	102.20
Sample C	90.09	90.79	100.78

* Mean average of three estimations.

electrochemical sensor showcased a high selectivity towards Azp detection.

5. Conclusion

In conclusion, we have illustrated an easy and successful synthesis of 5-carboxypolyindole decorated MoS_2 nanosheets for the development of an electro sensing platform as a modified glassy carbon electrode. This work offers a simple, cost-effective, and sensitive electroanalytical estimation of Azp in the biological sample without any cross-reactivity, false positives and matrix complications. The limit of detection was achieved to be as low as 74.65 nM. This method does not need any

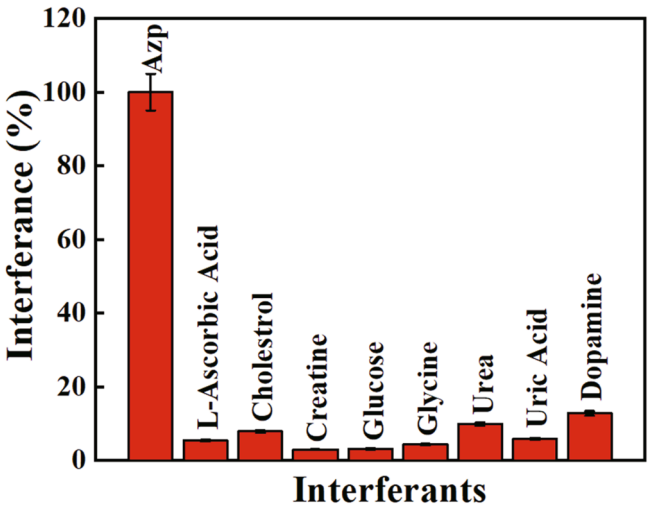

Fig. 5. Interference study. The x axis denotes the tested compounds and the y axis denotes the interference effect in percentage (%).

pretreatment of the sample. The ultra sensitivity of this nanomediator can be assigned to the immensely huge surface area, magnificent electrical conductivity and rapid electrode kinetics due to the electrocatalytic effect. Based on this sensing performance in PBS buffer and blood serum, it can be concluded that the present methodology has an immense potential to be effectively applied for the quantitative estimation of Azp in pharmaceutical formulations.

CRediT authorship contribution statement

Vineet Kumar Mall: Data curation, Writing – original draft, Investigation. **Ravi Prakash Ojha:** Investigation, Methodology, Writing – original draft. **Preeti Tiwari:** Investigation, Writing – review & editing. **Rajiv Prakash:** Supervision, Conceptualization, Writing – review & editing.

Declaration of Competing Interest

The authors declare that they have no known competing financial interests or personal relationships that could have appeared to influence the work reported in this paper.

Acknowledgements

Authors wish to express sincere gratitude to Prof. D. Dash, Institute of Medical Sciences, Banaras Hindu University, Varanasi for his utmost help in biological experiments. Authors are moreover thankful to CIF, IIT (BHU) for furnishing the instrumentation facilities. Vineet Kumar Mall and Ravi Prakash Ojha convey their acknowledgment to the UGC and IIT (BHU) for fellowship respectively.

Appendix A. Supplementary data

Supplementary data to this article can be found online at https://doi.org/10.1016/j.rechem.2022.100345.

References

[1] W. Rae, G. Burke, A. Pinto, A study of the utility of Azathioprine metabolite testing in myasthenia gravis, J. Neuroimmunol. 293 (2016) 82–85, https://doi.org/10.1016/j.jneuroim.2016.02.015.
[2] E. Asadian, A. Irajizad, S. Shahrokhian, Voltammetric studies of Azathioprine on the surface of graphite electrode modified with graphene nanosheets decorated with Ag nanoparticles, Mater. Sci. Eng. C 58 (2016) 1098–1104, https://doi.org/10.1016/j.msec.2015.09.022.
[3] H.L. McLeod, C. Siva, The thiopurine S-methyltransferase gene locus – implications for clinical pharmacogenomics, Pharmacogenomics 3 (2002) 89–98, https://doi.org/10.1517/14622416.3.1.89.
[4] T. Dervieux, R. Boulieu, Simultaneous determination of 6-thioguanine and methyl 6-mercaptopurine nucleotides of Azathioprine in red blood cells by HPLC, Clin. Chem. 44 (3) (1998) 551–555, https://doi.org/10.1093/clinchem/44.3.551.
[5] X.M. Muller, Drug immunosuppression therapy for adult heart transplantation. Part 1: immune response to allograft and mechanism of action of immunosuppressants, Ann. Thorac. Surg. 77 (2004) 354–362, https://doi.org/10.1016/j.athoracsur.2003.07.006.
[6] T.T. Fazio, A.K. Singh, E.R.M. Kedor-Hackmann, M.I.R. Miritello Santoro, Quantitative determination and sampling of Azathioprine residues for cleaning validation in production area, J. Pharm. Biomed. Anal. 43 (2007) 1495–1498, https://doi.org/10.1016/j.jpba.2006.10.016.
[7] K. Tsutsumi, Y. Otsuki, T. Kinoshita, Simultaneous determination of Azathioprine and 6-mercaptopurine in serum by reversed-phase high-performance liquid chromatography, J. Chromatogr. 231 (2) (1982) 393–399, https://doi.org/10.1016/s0378-4347 (00)81863-0.
[8] C.S. Lakshmi, M.N. Reddy, Spectrophotometric determination of Azathioprine in pharmaceutical formulations, Talanta 47 (1998) 1279–1286, https://doi.org/10.1016/S0039-9140(98)00216-1.
[9] A.H. Chalmers, A spectrophotometric method for the estimation of urinary Azathioprine, 6-mercaptopurine, and 6-thiouric acid, Biochem. Med. 12 (1975) 234–241, https://doi.org/10.1016/0006-2944 (75)90125-8.
[10] N.G. Göger, H.K. Parlatan, H. Basan, A. Berkkan, T. Özden, Quantitative determination of Azathioprine in tablets by 1H NMR spectroscopy, J. Pharm. Biomed. Anal. 21 (3) (1999) 685–689, https://doi.org/10.1016/S0731-7085 (99)00156-9.
[11] J. Wang, P. Zhao, S. Han, Direct determination of Azathioprine in human fluids and pharmaceutical formulation using flow injection chemiluminescence analysis, J. Chin. Chem. Soc. 59 (2012) 239–244, https://doi.org/10.1002/jccs.201100369.
[12] M. Govindasamy, S.-M. Chen, V. Mani, R. Devasenathipathy, R. Umamaheswari, K. J. Santhanaraj, A. Sathiyan, Molybdenum disulfide nanosheets coated multiwalled carbon nanotubes composite for highly sensitive determination of chloramphenicol in food samples milk, honey and powdered milk, J. Colld. Interface Sci. 485 (2017) 129–136, https://doi.org/10.1016/j.jcis.2016.09.029.
[13] P.M. Davadra, V.V. Mepal, M.R. Jain, C.G. Joshi, A.H. Bapodra, A validated UPLC method for the determination of process related impurities in Azathioprine bulk drug, Anal. Methods 3 (2011) 198–204, https://doi.org/10.1039/C0AY00406E.
[14] S. Kulkarni, K. Chitalkar, N. Shinde, P. Tekale, R. Lanjewar, A validated high performance thin-layer chromatographic method for the determination of Azathioprine from pharmaceutical formulation, JPC: J. Planar Chromat.-Mod.TLC 27 (2014) 120–123, https://doi.org/10.1556/JPC.27.2014.2.9.
[15] S.P. Chen, Z. Qiao, A. Vivon, C.M. Hosten, Determination of the orientation of Azathioprine adsorbed on a silver electrode by SERS and ab initio calculations, Spectrochim. Acta A 59 (2003) 2905–2914, https://doi.org/10.1016/S1386-1425(03)00099-4.
[16] A. Shafaati, B.J. Clark, Determination of Azathioprine and its related substances by capillary zone electrophoresis and its application to pharmaceutical dosage forms assay, Drug Dev. Ind. Pharm. 26 (2000) 267–273, https://doi.org/10.1081/DDC-100100355.
[17] C.S.P. Sastry, K.R. Srinivas, K.M.M.K. Prasad, Spectrophotometric determination of drugs in pharmaceutical formulations with N-bromosuccinimide and Celestine blue, Microchim. Acta 122 (1-2) (1996) 77–86.
[18] P. Tiwari, A. Kumar, R. Prakash, Electrochemical detection of azidothymidine on modified probes based on chitosan stabilized silver nanoparticles hybrid material, RSC Adv. 5 (2015) 90089–90097, https://doi.org/10.1039/C5RA15908C.
[19] S.E. Baghbamidi, H. Beitollahi, S. Tajik, R. Hosseinzadeh, Voltammetric sensor based on 1-benzyl-4-ferrocenyl-1*H*-[1, 2, 3]-triazole/carbon nanotube modified glassy carbon electrode; detection of hydrochlorothiazide in the presence of propranolol, Int. J. Electrochem. Sci. 11 (2016) 10874–10883, https://doi.org/10.20964/2016.12.92.
[20] S. Tajik, H. Beitollahi, A sensitive chlorpromazine voltammetric sensor based on graphene oxide modified glassy carbon electrode, Anal. Bioanal. Chem. Res. 6 (2019) 171–182, https://doi.org/10.22036/ABCR.2018.89229.1154.
[21] Y. Meng, L. Aldous, S.R. Belding, R.G. Compton, The formal potentials and electrode kinetics of the proton/hydrogen couple in various room temperature ionic liquids, Chem. Commun. 48 (2012) 5572–5574, https://doi.org/10.1039/C2CC31402A.
[22] M.A. Rashed, M. Faisal, M. Alsaiari, S.A. Alsareii, F.A. Harra, MWCNT-doped polypyrrole-carbon black modified glassy carbon electrode for efficient electrochemical sensing of nitrite ions, Electrocatalysis 12 (2021) 650–666, https://doi.org/10.1007/s12678-021-00675-6.
[23] A. Mehrabi, M. Rahimnejad, M. Mohammadi, M. Pourali, Electrochemical detection of Flutamide as an anticancer drug with gold nanoparticles modified glassy carbon electrode in the presence of prostate cancer cells, J. Appl. Electrochem. 51 (2021) 597–606, https://doi.org/10.1007/s10800-020-01519-9.
[24] S.A. Alkahtani, A.M. Mahmoud, M.M. El-Wekil, Electrochemical sensing of copper-chelator D- penicillamine based on complexation with gold nanoparticles modified copper based-metal organic frameworks, J. Electroanal. Chem. 908 (2022), 116102, https://doi.org/10.1016/j.jelechem.2022.116102.
[25] S. Guo, D. Wen, Y. Zhai, S. Dong, E. Wang, Platinum nanoparticle ensemble-on-graphene hybrid nanosheet: one-pot, rapid synthesis, and used as new electrode material for electrochemical sensing, ACS Nano 4 (2010) 3959–3968, https://doi.org/10.1021/nn100852h.

[26] S. Nikhil, A. Karthika, P. Suresh, A. Suganthi, M. Rajarajan, A selective and sensitive electrochemical determination of catechol based on reduced graphene oxide decorated β-cyclodextrin nanosheet modified glassy carbon electrode, Adv. Powder Technol. 32 (2021) 2148–2159, https://doi.org/10.1016/j.apt.2021.04.027.

[27] S. Immanuel, R. Sivasubramanian, Electrochemical studies of NADH oxidation on chemically reduced graphene oxide nanosheets modified glassy carbon electrode, Mater. Chem. Phys. 249 (2020), 123015, https://doi.org/10.1016/j.matchemphys.2020.123015.

[28] J.F. Guan, J. Zou, Y.P. Liu, X.Y. Jiang, J.G. Yu, Hybrid carbon nanotubes modified glassy carbon electrode for selective, sensitive and simultaneous detection of dopamine and uric acid, Ecotoxicol. Environ. Safety 201 (2020), 110872, https://doi.org/10.1016/j.ecoenv.2020.110872.

[29] S. Ostovar, S. Maghsoudi, M. Mousavi, Development of a sensitive voltammetric sensor for diltiazem determination in biological samples using MWCNT/PPy-PBA modified glassy carbon electrode, Synth. Metals 281 (2021), 116928, https://doi.org/10.1016/j.synthmet.2021.116928.

[30] M. Regiart, S.V. Pereira, V. Spotorno, F.A. Bertolino, J. Raba, Nanostructured voltammetric sensor for ultra-trace anabolic drug determination in food safety field, Sens. Actuators B: Chem. 188 (2013) 1241–1249, https://doi.org/10.1016/j.snb.2013.07.117.

[31] G. Gedda, S. Pandey, M.L. Bhaisare, H.-F. Wu, Carbon dots as nanoantennas for anti-inflammatory drug analysis using surface-assisted laser desorption/ionization time-of-flight mass spectrometry in serum, RSC Adv. 4 (72) (2014) 38027–38033.

[32] X. Zhang, Z. Lai, C. Tan, H. Zhang, Solution-processed two-dimensional MoS_2 nanosheets: preparation, hybridization, and applications, Angew. Chem. Int. Ed. 55 (2016) 8816–8838, https://doi.org/10.1002/anie.201509933.

[33] D. Zhang, Z. Yang, P. Li, M. Pang, Q, Xue, Flexible self-powered high-performance ammonia sensor based on Au-decorated $MoSe_2$ nanoflowers driven by single layer MoS_2-flake piezoelectric nanogenerator, Nano Energy 65 (2019), https://doi.org/10.1016/j.nanoen.2019.103974.

[34] Y. Zeng, Z. Shen, X. Wu, D.X. Wang, Y.L. Wang, Y.L. Sun, L. Wu, Y. Zhang, Back contact modification of the optoelectronic device with transition metal dichalcogenide VSe_2 film drives solar cell efficiency, J. Materiomics 7 (2021) 470–477, https://doi.org/10.1016/j.jmat.2020.11.008.

[35] R.K. Upadhyay, S. Naskar, N. Bhaskar, S. Bose, B. Basu, Modulation of protein adsorption and cell proliferation on polyethylene immobilized graphene oxide reinforced HDPE bionanocomposites, ACS Appl. Mater. Interfaces 8 (19) (2016) 11954–11968, https://doi.org/10.1021/acsami.6b00946.

[36] D. Zhang, J. Wu, P. Li, Y. Cao, Room-temperature SO_2 gas-sensing properties based on a metal-doped MoS_2 nanoflower: an experimental and density functional theory investigation, J. Mater. Chem. A 5 (2017) 20666–20677, https://doi.org/10.1039/C7TA07001B.

[37] X. Gan, H. Zhao, X. Quan, Two-dimensional MoS_2: a promising building block for biosensors, Biosens. Bioelectronics 89 (2017) 56–71, https://doi.org/10.1016/j.bios.2016.03.042.

[38] R. Sha, T.K. Bhattacharyya, MoS_2-based nanosensors in biomedical and environmental monitoring applications, Electrochim. Acta 249 (2020), 136370, https://doi.org/10.1016/j.electacta.2020.136370.

[39] Y. Wang, B. Zhang, Y. Tang, F. Zhao, B. Zeng, Fabrication and application of a rutin electrochemical sensor based on rose-like AuNPs-MoS_2-GN composite and molecularly imprinted chitosan, Microchem. J. 168 (2021), 106505, https://doi.org/10.1016/j.microc.2021.106505.

[40] Y. Fadil, V. Agarwal, F. Jasinski, S.C. Thickett, H. Minami, P.B. Zetterlund, Electrically conductive polymer/rGO nanocomposite films at ambient temperature via miniemulsion polymerization using GO as surfactant, Nanoscale 11 (2019) 6566–6570, https://doi.org/10.1039/C9NR00816K.

[41] S.P. Selvam, S.R. Chinnadayyala, S. Cho, Electrochemical nanobiosensor for early detection of rheumatoid arthritis biomarker: Anti- cyclic citrullinated peptide antibodies based on polyaniline (PANI)/MoS2-modified screen-printed electrode with PANI-Au nanomatrix-based signal amplification, Sens. Actuators B: Chem 333 (2021), 129570, https://doi.org/10.1016/j.snb.2021.129570.

[42] H. Tang, J. Wang, H. Yin, H. Zhao, D. Wang, Z. Tang, Growth of polypyrrole ultrathin films on MoS_2 monolayers as high-performance supercapacitor electrodes, Adv. Mater. 27 (6) (2014) 1117–1123, https://doi.org/10.1002/adma.201404622.

[43] V. Raju, V.N. Kumar Y, V.R. Jetti, P. Basak, MoS 2/polythiophene composite cathode as a potential host for rechargeable aluminum batteries: deciphering the impact of processing on the performance, ACS Appl. Energy Mater. 4 (9) (2021) 9227–9239, https://doi.org/10.1021/acsaem.1c01480.

[44] R. Mishra, N.R. Nirala, R.K. Pandey, R.P. Ojha, R. Prakash, Homogenous dispersion of MoS2 nanosheets in polyindole matrix at air-water interface assisted by Langmuir technique, Langmuir 33 (47) (2017) 13572–13580, https://doi.org/10.1021/acs.langmuir.7b03019.

[45] L. Joshi, B. Gupta, R. Prakash, Chemical synthesis of poly(5-carboxyindole) and poly(5-carboxyindole)/carboxylated multiwall carbon nanotube nanocomposite, Thin Solid Films 519 (2010) 218–222, https://doi.org/10.1016/j.tsf.2010.07.123.

[46] T.N.Y. Khawula, K. Raju, P.J. Franklyn, I. Sigalas, K.I. Ozoemena, Symmetric pseudocapacitors based on molybdenum disulfide (MoS_2)-modified carbon nanospheres: correlating physicochemistry and synergistic interaction on energy storage, J. Mater. Chem. A 4 (2016) 6411–6425, https://doi.org/10.1039/c6ta00114a.

[47] L. Joshi, R. Prakash, Synthesis of conducting poly(5-carboxyindole)/Au nanocomposite: investigation of structural and nanoscale electrical properties, Thin Solid Films 534 (2013) 120–125, https://doi.org/10.1016/j.tsf.2013.02.025.

[48] J. Han, G. Xu, B. Ding, J. Pan, H. Dou, D.R. MacFarlane, Porous nitrogen-doped hollow carbon spheres derived from polyaniline for high performance supercapacitors, J. Mater. Chem. A 2 (2014) 5352–5357, https://doi.org/10.1039/c3ta15271e.

[49] J. Wang, Q. Zhao, H. Hou, Y. Wu, W. Yu, X. Ji, L. Shao, Nickel nanoparticles supported on nitrogen-doped honeycomb-like carbon frameworks for effective methanol oxidation, RSC Adv. 7 (2017) 14152–14158, https://doi.org/10.1039/c7ra00590c.

[50] Z. Xing, Z. Ju, Y. Zhao, J. Wan, Y. Zhu, Y. Qiang, Y. Qian, One-pot hydrothermal synthesis of Nitrogen-doped graphene as high-performance anode materials for lithium ion batteries, Sci. Rep. 6 (26146) (2016), https://doi.org/10.1038/srep26146.

[51] L. Zhao, J. Jia, Z. Yang, J. Yu, A. Wang, Y. Sang, W. Zhou, H. Liu, One-step synthesis of CdS nanoparticles/MoS_2 nanosheets heterostructure on porous molybdenum sheet for enhanced photocatalytic H_2 evolution, Appl. Catal. B 210 (2017) 290–296, https://doi.org/10.1016/j.apcatb.2017.04.003.

[52] D. Briggs, C.D. Wagner, W.M. Riggs, L.E. Davis, J.F. Moulder, G.E. Muilenberg, Handbook of X-ray Photoelectron Spectroscopy, Perkin-Elmer Corp., Physical Electronics Division, Eden Prairie, Minnesota, USA, 1979, pp 190, Surface Interface Anal. 3(4) (1981), https://doi.org/10.1002/sia.740030412.

[53] S. Shahrokhian, M. Ghalkhani, Electrochemical study of Azathioprine at thin carbon nanoparticle composite film electrode, Electrochem. Commun. 11 (2009) 1425–1428, https://doi.org/10.1016/j.elecom.2009.05.025.

[54] J.M. Zen, J.J. Jou, A.S. Kumar, A sensitive voltammetric method for the determination of parathion insecticide, Anal. Chim. Acta 396 (1999) Issue 39-44, https://doi.org/10.1016/S0003-2670(99)00357-8.

[55] J.C. Chen, J.L. Shih, C.H. Liu, M.Y. Kuo, J.M. Zen, Disposable electrochemical sensor for determination of nitroaromatic compounds by a single-run approach, Anal. Chem. 78 (11) (2006) 3752–3757, https://doi.org/10.1021/ac060002n.